THERMO FLUID DYNAMICS OPTIMISATION OF TAPERED HELICALLY-COILED SOLAR THERMAL COLLECTORS

S. Landini[1*], F. Ghani[2], T.S. O'Donovan[3]

[1]School of Engineering, University of East Anglia, Norwich NR4 7TJ, UK
[2]SolarisKit Ltd, Michelin Scotland Innovation Parc, Dundee DD4 8UQ, UK
[3]School of Engineering and Physical Sciences, Heriot-Watt University, Edinburgh EH14 4AS, UK

ABSTRACT

This study investigated the effect of the absorber geometry on the heat transfer performance of a novel low-cost flat-packable tapered helically-coiled solar thermal collector under laminar flow conditions. Importantly, the potential heat transfer enhancement by secondary Dean flows was evaluated. A computational fluid dynamics (CFD) model was developed and validated with experimental data found in the literature. Overall results show that the Nusselt number increases with the Helical number along the tube. However, this difference is only appreciable close to the end of the tube but quite negligible. The collector geometry should therefore be optimised in terms of optical efficiency to maximise the intercepted solar irradiance on the absorber surface.

1. INTRODUCTION

Evidence shows that hot water accounts for up to 70% of domestic electricity consumption in African countries [1,2], posing constant stress on the electricity grid. This demand, however, could be met using solar thermal collectors. Although this technology is mature, its implementation has been limited in Africa due to high costs, difficult transportation, and complex installation [2].

To address these issues, a novel low-cost flat-packable tapered helically-coiled solar thermal collector (Figure 1) has been developed by SolarisKit Ltd. The collector comprises a tube (absorber) helically coiled around a vertical structure and tapered in a conical shape. The absorber is located within a pyramidal enclosure with a base reflective mirror which reflects part of the sun rays that are not directly absorbed by the tube.

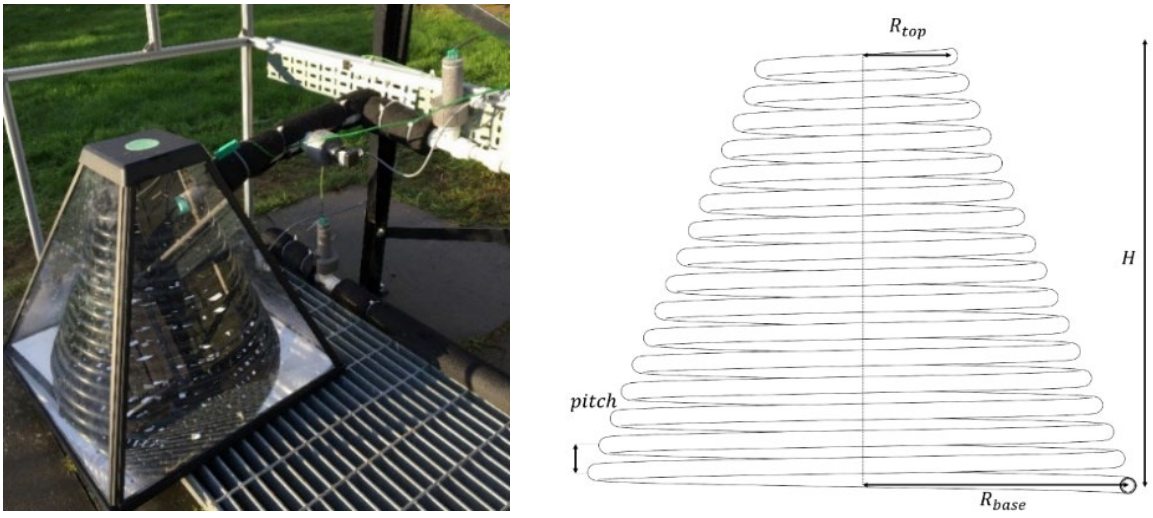

Figure 1: Novel low-cost flat-packable tapered helically-coiled solar thermal collector.

*Corresponding Author: s.landini@uea.ac.uk

This study aimed to investigate the effect of the absorber geometry (Figure 1, right) on the heat transfer performance of the collector. Importantly, the potential heat transfer enhancement by secondary Dean flows [3] was evaluated. To do so, a computational fluid dynamics (CFD) model was developed and validated with experimental data found in the literature.

2. METHODOLOGY

A CFD model of a tapered helically-coiled tube heat exchanger was developed in Ansys 2019R3. The effect of the average non-dimensional pitch ($\gamma = \frac{p}{2\pi R}$), contraction ($c = \frac{R_{top}}{R_{base}}$), and base coil radius (R_{base}) have been investigated for a laminar steady-state flow regime (water mass flow rate $\dot{m}$=0.01 kg/s, water inlet Reynolds number Re=1058) typical of this specific application. It must be mentioned that solar thermal collectors' water flow rates are kept low (e.g. 0.5-1 L/min) to gain useful temperature rises.

The model proposed simulates the thermo-fluid dynamics of the collector introducing a uniform volumetric heat generation rate to emulate the absorbed solar irradiance. This allows to include the effect of the tube heat conduction and the heat dissipation by convention from the tube external surface towards the surroundings. This translates into a non-uniform decreasing heat flux along the tube internal surface.

The model included a water body and a tube body. The latter was divided into an internal passive body (Figure 2, left, grey) of 1mm thickness and an external fictitious body (called “film”, Figure 2, left, red) of 0.5mm thickness. The film emulates the tube external layer where the incident solar irradiance is absorbed and converted into heat. The mesh was developed in Ansys Mesh (Figure 2, right). The results sensitivity to the mesh quality has been conducted and independency confirmed.

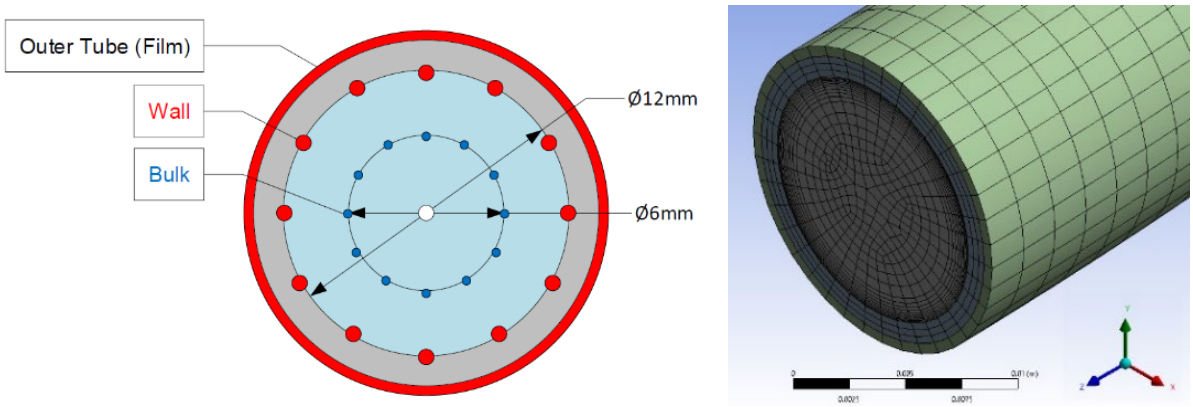

Figure 2: Left: sampling points on the cross-section of the tube: 12 on the wall, 12 on the circumference equally distanced from the wall and the centre (bulk), and 1 at the centre. Right: mesh, view of the inlet section. Method: 2mm quadrilateral sweep method, 10-layer inflation at the water-tube interface, 3-layer tube body, 1-layer film, edges size of 1mm.

Ansys default thermo-physical properties were assumed constant for both water and tube, except for the water density, taken as a function of temperature to account for buoyancy motion due to gravity. The momentum and energy equations were solved for a laminar steady-state flow. The solution method was a pressure-based segregated SIMPLEC with spatial discretisation methodology based on Green-Gauss Node (gradient), PREssure STaggering Option (pressure), and Second Order (energy and momentum). Convergence was defined by a condition of absolute residuals lower than 10^{-6} for momentum and energy and 10^{-3} for continuity, and stable values of key parameters. The CFD model was successfully validated against experimental data for forced convection laminar heat transfer within straight pipes [4,5] and helically-coiled pipes [6] with median RMSE below 5% and 6% respectively.

3. RESULTS

All geometries simulated shared the same tube total length L=17m, internal radius r=6mm, and thickness t=1.5mm. The following boundary conditions were applied:

- water mass flow rate of 0.01 kg/s
- water inlet temperature of 300K
- water outlet pressure of 0 Pa
- uniform film volumetric heat generation rate of 2.066 mW/m^3 (equal to an external heat flux of 1000 W/m^2)
- ideal thermal contact between bodies, external convection characterised by a uniform heat transfer coefficient of 10 W/m^2, and ambient temperature of 283K.

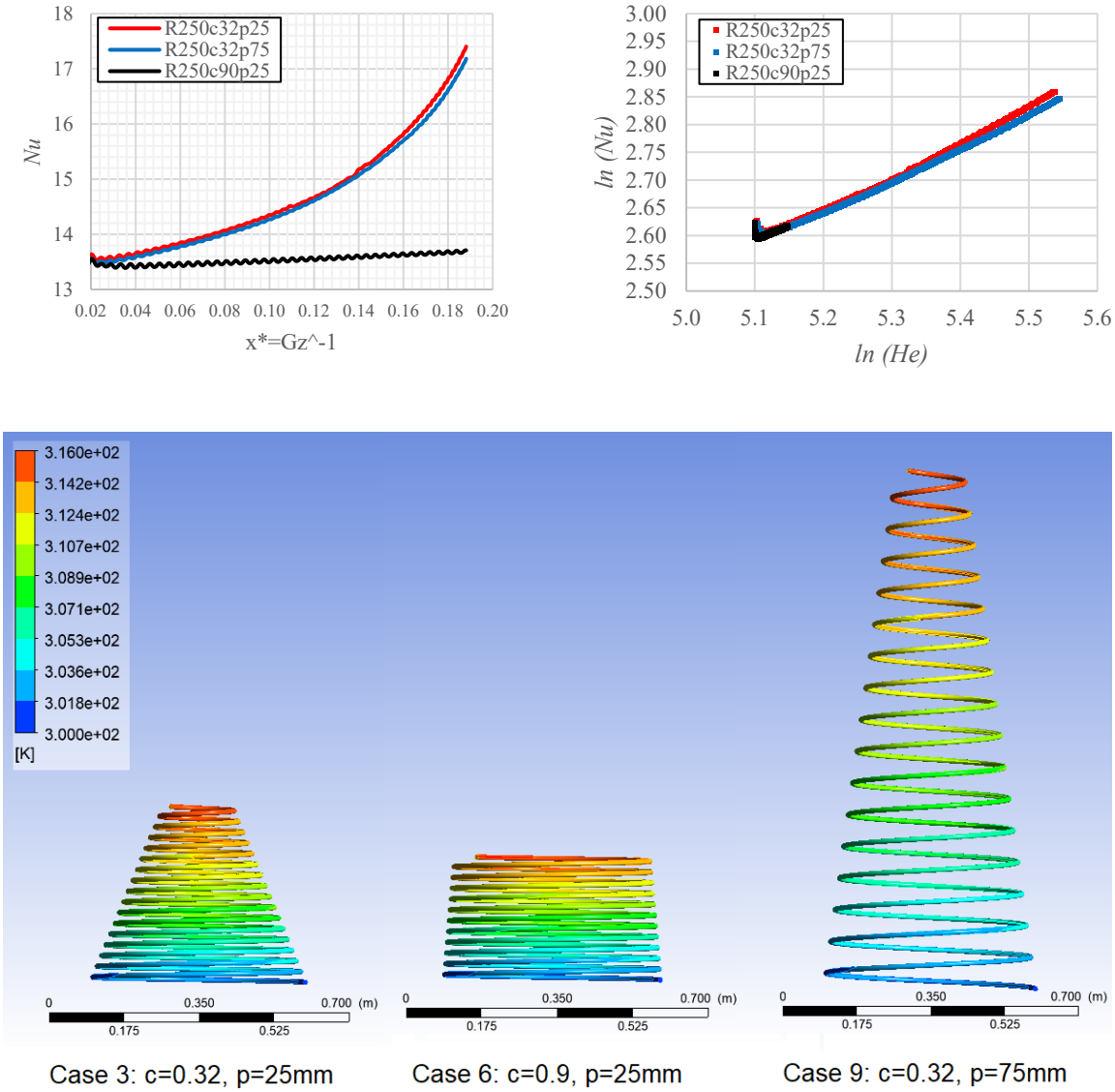

Figure 3: Nusselt number for three chosen cases. Upper left: variation along the non-dimensional tube axial length x* (inverse of Graetz number defined as $Gz = \frac{d\,Re\,Pr}{x}$). Upper right: *ln(Nu)* vs *ln(He)*. By linear regression of all data points, a power law was identified: $Nu = a \cdot He^b$, with a=1.236, b=0.467, and R^2=0.99. Bottom: temperature profiles.

The overall performance of all geometries tested (13 in total) is shown in Table 1 in comparison with a straight pipe (S). Useful parameters such as average non-dimensional pitch (γ), average Dean number ($De = Re\sqrt{\frac{r}{R}}$), and average Helical number ($He = \frac{De}{1-\gamma^2}$) are also reported. In addition, 25 polylines were defined (Figure 2 left) to sampled temperature and heat flux values at 1,000 equally-distanced points along the tube and Nusselt numbers were calculated, as reported in Figure 3 for three chosen cases.

Table 1: Overall Results. Cases are sorted from higher to lower outlet temperatures. Dean number (*De*), non-dimensional pitch (γ), and Helical number (*He*) are calculated from the average coil radius (*R*), contraction ratio (*c*), and curvature ($\frac{r}{R}$).

Case	R_{base}	c	p	H	De	γ	He	Δp	T_{out}	Q	Q/P
-	[mm]	-	[mm]	[mm]	-	-	-	[Pa]	[K]	[W]	-
1	100	0.32	25	1023	318.96	0.060	320.12	775	314.03	586.71	5.499E+04
2	250	0.32	75	1227	201.73	0.072	202.79	661	313.81	577.51	6.341E+04
3	250	0.32	100	1632	201.73	0.096	203.62	633	313.73	574.18	6.584E+04
4	250	0.7	25	318	177.76	0.019	177.82	613	313.71	573.43	6.790E+04
5	250	1	25	271	163.88	0.016	163.92	599	313.71	573.32	6.947E+04
6	250	0.9	25	285	168.14	0.017	168.19	602	313.71	573.20	6.918E+04
7	250	0.32	50	819	201.73	0.048	202.20	622	313.70	573.05	6.684E+04
8	300	0.32	25	342	184.15	0.020	184.22	617	313.70	572.99	6.741E+04
9	250	0.5	25	361	189.24	0.021	189.32	627	313.70	572.85	6.637E+04
10	500	0.32	25	205	142.64	0.012	142.66	581	313.70	572.78	7.161E+04
11	250	0.32	25	410	201.73	0.024	201.84	640	313.69	572.49	6.498E+04
12	200	0.32	25	512	225.54	0.030	225.74	669	313.68	572.10	6.211E+04
13	400	0.32	25	256	159.48	0.015	159.51	593	313.65	570.98	6.986E+04
S	-	-	-	-	-	-	-	181	313.58	567.75	2.279E+05

The variation of the key performance indices is limited, leading to the statistics across all 13 cases reported in Table 2. Interestingly, the effect of the pitch (cases 3, 8, 9, 10) is found to be similar to a study by Sheeba et al. [6] where a variation of the coil pitch p (in their study in absence of contraction) from 25mm to 150mm lead to a variation of the overall heat transfer coefficient lower than 3% (lower than 1% in this study) and an apparent maximum for a pitch equal to 75mm (same for this study).

The sensitivity of the water overall heating rate to pitch (p), base radius (R_b), and contraction ratio (c) is also reported in Figure 4. Even if the variation is minimal, an increase in pitch, a decrease in base radius, and an increase in contraction ratio lead to higher average Dean numbers, Helical numbers, and therefore better heat transfer rates.

Table 2: Overall Results Statistics

	Δp [Pa]	q_{wall} [W/m^2]	T_{out} [K]	T_{ext} [K]	T_{wall} [K]	Q [W]	P [W]	Q/P	η_{th}
Min	581	891.91	313.65	310.75	308.06	571	8.00E-03	5.50E+04	71.42%
Max	775	918.09	314.03	311.06	308.36	587	1.07E-02	7.16E+04	73.38%
Average	633	897.31	313.73	310.90	308.22	574	8.72E-03	6.62E+04	71.83%
Median	622	895.32	313.70	310.91	308.25	573	8.57E-03	6.68E+04	71.68%
SD	50	6.699	0.096	0.084	0.094	4.020	6.82E-04	4.27E+03	0.50%
	7.95%	0.75%	0.03%	0.03%	0.03%	0.70%	7.95%	6.39%	0.70%

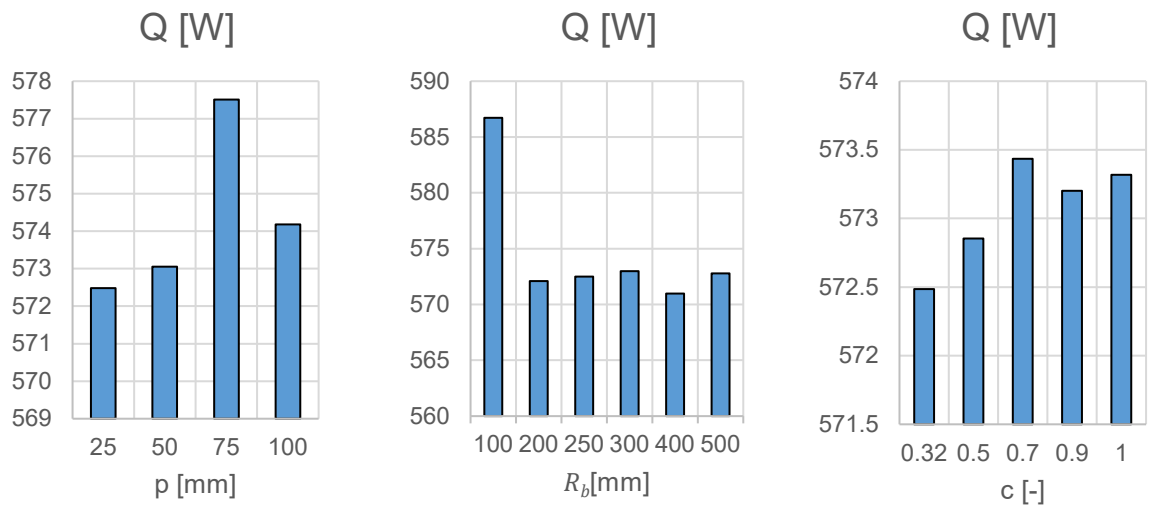

Figure 4: Sensitivity of the overall water heating rate to pitch (p), base radius (R_b), and contraction ratio (c)

In addition, to further validate the results, correlations (reported in Table 3) for fully-developed laminar-flow heat transfer of helically-coiled tube (without contraction c) for an iso-heat flux boundary condition proposed by Janssen and Hoogendorn [7], Manlapaz and Churchill [8], and Xin and Ebadian [9] are used to calculate the Nusselt number for each case at the 1,000 points along the pipe and compared them with the current model results. To be consistent with the studies definition of Nusselt number, the average local heat transfer coefficient h_x is here defined (refer to Figure 2) as the ratio between the average local heat flux q_x (calculated from the 12 wall values $q_{x,i}$) and the difference between the average local wall temperature $T_{w,x}$ (calculated from the 12 wall values $T_{w,x,i}$) and local bulk temperature $T_{b,x}$ (calculated from the 12 bulk values $T_{b,x,i}$ and the centre value $T_{c,x}$).

Table 3: Average Nusselt number correlations for fully-developed laminar-flow heat transfer of helically-coiled tube (without contraction) for an iso-heat flux boundary condition

Authors	Ref.	Year	Iso-flux Nu Correlation	Validity
Janssen & Hoogendorn	[7]	1978	$Nu = 0.7\, Re^{0.43} Pr^{1/6} \delta^{0.07}$, $\delta = \frac{d}{D}$	$100 < De < 830$
Manlapaz & Churchill	[8,10]	1981	$Nu = \left\{ \left\{ 3.657 + \frac{4.343}{\left[1 + \frac{957}{\mathrm{Pr}\, De^2}(1+\gamma^2)\right]^2} \right\}^3 + 1.158 \left\{ \frac{De}{\left[1 + \frac{0.477}{Pr}\right](1+\gamma^2)^{0.5}} \right\}^{3/2} \right\}^{\frac{1}{3}}$	$De < 2000$ $0.8 < De\,(1+\gamma^2)^{0.5} < 2000$
Xin & Ebadian	[9]	1997	$Nu = (2.153 + 0.318\, De^{0.63})\, Pr^{0.177}$	$20 < De < 2000$ $0.7 < Pr < 175$ $0.0267 < \delta = \frac{d}{D} < 0.0884$

Overall, the results of the current model for all cases simulated in this study are in line with the proposed correlations. Interestingly, the Nusselt number appears to better agree with the correlation by Manlapaz & Churchill [8,10], which is the only one including the effect of the non-dimensional pitch γ. In addition, the relative RMSE of the Nusselt number calculated from the CFD model compared to the Manlapaz & Churchill correlation for all cases is in the range of 5.83%-6.37%.

4. CONCLUSIONS

Overall, the Nusselt number increases with the Helical number along the tube, especially for geometries characterised by lower *c* independently from the pitch. However, this difference is only appreciable close to the end of the tube and the overall thermo-fluid dynamics performance of all geometries tested are not strongly dissimilar. The collector geometry should therefore be optimised in terms of optical efficiency.

ACKNOWLEDGEMENTS

The authors would like to thank Innovate UK for supporting this project.

REFERENCES

[1] IRENA, Africa 2030: Roadmap for a Renewable Energy Future, 2015. www.irena.org/remap.

[2] IEA, Africa Energy Outlook 2019, 2019. https://www.iea.org/reports/africa-energy-outlook-2019.

[3] W.R. Dean, J.M. Hurst, Note on the Motion of Fluid in Curved Pipe, 6 (2020) 77–85.

[4] S.W. Churchill, H. Ozoe, Correlations for Laminar Forced Convection in Flow Over a Uniformly Heated Plate and in Developing and Fully Developed Flow in a Tube., J. Heat Transfer. 95 (1973) 78–84.

[5] R. Clarke, D.P. Finn, The influence of secondary refrigerant air chiller U-bends on fluid temperature profile and downstream heat transfer for laminar flow conditions, Int. J. Heat Mass Transf. 51 (2008) 724–735. https://doi.org/10.1016/j.ijheatmasstransfer.2007.04.047.

[6] A. Sheeba, C.M. Abhijith, M. Jose Prakash, Experimental and numerical investigations on the heat transfer and flow characteristics of a helical coil heat exchanger, Int. J. Refrig. 99 (2019) 490–497. https://doi.org/10.1016/j.ijrefrig.2018.12.002.

[7] L.A.M. Janssen, C.J. Hoogendoorn, Laminar convective heat transfer in helical coiled tubes, Int. J. Heat Mass Transf. 21 (1978) 1197–1206. https://doi.org/10.1016/0017-9310(78)90138-2.

[8] R.L. Manlapaz, S.W. Churchill, Fully developed laminar convection from a helical coil, Chem. Eng. Commun. 9 (1981) 185–200. https://doi.org/10.1080/00986448108911023.

[9] R.C. Xin, M.A. Ebadian, The effects of Prandtl numbers on local and average convective heat transfer characteristics in helical pipes, J. Heat Transfer. 119 (1997) 467–473. https://doi.org/10.1115/1.2824120.

[10] M.S. El-Genk, T.M. Schriener, A Review and Correlations for Convection Heat Transfer and Pressure Losses in Toroidal and Helically Coiled Tubes, Heat Transf. Eng. 38 (2017) 447–474. https://doi.org/10.1080/01457632.2016.1194693.